The Structure of Coronal Mass Ejections Recorded by the K-Coronagraph at Mauna Loa Solar Observatory

Hongqiang Song,[1] Leping Li,[2] Zhenjun Zhou,[3] Lidong Xia,[1] Xin Cheng,[4] and Yao Chen[1,5]

[1]*Shandong Provincial Key Laboratory of Optical Astronomy and Solar-Terrestrial Environment, and Institute of Space Sciences, Shandong University, Weihai, Shandong 264209, China*
[2]*National Astronomical Observatories, Chinese Academy of Sciences, Beijing, 100101, China*
[3]*School of Atmospheric Sciences, Sun Yat-sen University, Zhuhai, Guangdong 519000, China*
[4]*School of Astronomy and Space Science, Nanjing University, Nanjing, Jiangsu 210093, China*
[5]*Institute of Frontier and Interdisciplinary Science, Shandong University, Qingdao, Shandong 266237, China*

ABSTRACT

Previous survey studies reported that coronal mass ejections (CMEs) can exhibit various structures in white-light coronagraphs, and ∼30% of them have the typical three-part feature in the high corona (e.g., 2–6 $R_\odot$), which has been taken as the prototypical structure of CMEs. It is widely accepted that CMEs result from eruption of magnetic flux ropes (MFRs), and the three-part structure can be understood easily by means of the MFR eruption. It is interesting and significant to answer why only ∼30% of CMEs have the three-part feature in previous studies. Here we conduct a synthesis of the CME structure in the field of view (FOV) of K-Coronagraph (1.05–3 $R_\odot$). In total, 369 CMEs are observed from 2013 September to 2022 November. After inspecting the CMEs one by one through joint observations of the AIA, K-Coronagraph and LASCO/C2, we find 71 events according to the criteria: 1) limb event; 2) normal CME, i.e., angular width ≥ 30°; 3) K-Coronagraph caught the early eruption stage. All (or more than 90% considering several ambiguous events) of the 71 CMEs exhibit the three-part feature in the FOV of K-Coronagraph, while only 30–40% have the feature in the C2 FOV (2–6 $R_\odot$). For the first time, our studies show that 90–100% and 30–40% of normal CMEs possess the three-part structure in the low and high corona, respectively, which demonstrates that many CMEs can lose the three-part feature during their early evolutions, and strongly supports that most (if not all) CMEs have the MFR structures.

Keywords: Solar coronal mass ejections − Solar filament eruptions − magnetic reconnection

1. INTRODUCTION

On 1971 September 29, the first orbiting white-light coronagraph (Koomen et al. 1975) was launched on Orbiting Solar Observatory Number 7 (Follett et al. 1974), and the coronagraph recorded the first images of a coronal mass ejection (CME) on 1971 December 14 (Tousey 1973). From that time onwards, CMEs have been a subject of intense investigation in solar physics (Chen 2011; Webb & Howard 2012). Theoretically, CMEs originate from eruption of magnetic flux ropes (MFRs), which can form prior to (Low 2001; Patsourakos et al. 2013; Song et al. 2015a; Kliem et al. 2021) and during (Song et al. 2014; Ouyang et al. 2015; Wang et al. 2017; Jiang et al. 2021) solar eruptions.

In general, hot channels and coronal cavities are regarded as the proxies of MFRs in active regions (Zhang et al. 2012; Song et al. 2015a) and quiet-Sun regions (Wang & Stenborg 2010; Chen et al. 2018), respectively. The MFR can provide support to the prominence against gravity (e.g., Yan et al. 2016). Therefore, CMEs are usually associated with eruptions of hot channels (high-temperature ejecta) (Zhang et al. 2012; Cheng et al. 2013; Song et al. 2015b), coronal cav-

Corresponding author: Hongqiang Song
hqsong@sdu.edu.cn

ities (middle-temperature ejecta) (Gibson et al. 2006; Forland et al. 2013; Song et al. 2022), and/or prominences (low-temperature ejecta) (Gopalswamy et al. 2003; Li et al. 2012; Song et al. 2018; Zhou et al. 2023a,b) observationally.

The white-light coronagraph on the Solar Maximum Mission satellite recorded a CME with three-part structure on 1980 August 5, i.e., a bright core within a dark cavity surrounded by a bright loop front (Illing & Hundhausen 1985) that included the low coronal observations of the CME from Mauna Loa MK3 coronameter. Since then, the three-part structure has become the prototypical structure of CMEs (e.g., Howard 2006) though only $\sim$30% of CMEs exhibit the three-part feature in the high corona, e.g., 2–6 $R_\odot$. In several decades, it is widely accepted that the bright front originates from the plasma pileup along the MFR boundary, the cavity represents the MFR, and the bright core corresponds to the prominence (e.g., Vourlidas et al. 2013).

However, recent studies pointed out that the traditional opinion is questionable, because some three-part CMEs are not associated with prominence eruptions at all (Howard et al. 2017; Song et al. 2017, 2019b, 2023; Wang et al. 2022). Based on dual-viewpoint and seamless observations from the inner to outer corona, a new explanation on the three-part nature has been proposed, in which the bright frontal loop is formed due to the compression as the magnetic loops are successively pushed to stretch up by the underlying MFR (Low 2001; Chen 2009), the core can correspond to the MFR and/or prominence, and the dark cavity between the CME front and the MFR is a low-density zone with sheared magnetic field (Song et al. 2017, 2019a). Recent observations clearly demonstrated that both hot channels (Song et al. 2023) and coronal cavities (Song et al. 2022) evolved into the bright core of three-part CMEs.

The new explanation also points out that CMEs can lose the three-part feature gradually when propagating outwards, because the dark cavity vanishes due to the MFR expansion and growth through magnetic reconnections, and/or because the bright core fades away due to the prominence expansion and drainage (Song et al. 2023). This answers why only a portion of CMEs have the prototypical structure in previous survey studies (e.g., Vourlidas et al. 2013). As mentioned, CMEs result from MFR eruption, thus the new explanation predicts that all normal CMEs possess the three-part structure in the low corona, i.e., in the early eruption stage. Here the normal CMEs do not include the narrow ones with angular width less than 30° for two factors: 1) the narrow events might be jets, instead of CMEs with small angular width; 2) to observe the structure of narrow CMEs, coronagraphs with higher spatial resolution are necessary.

To examine whether all normal CMEs have the three-part structure in the early eruption stage, we conduct a survey study based on observations of the coronal solar magnetism observatory (COSMO) K-coronagraph (K-COR) from 2013 September to 2022 November. The paper is organized as follows. Section 2 introduces the related instruments and Methods. The observations and results are displayed in Section 3, which is followed by a summary and discussion in the final section.

2. INSTRUMENTS AND METHODS

The Atmospheric Imaging Assembly (AIA) (Lemen et al. 2012) on board the Solar Dynamics Observatory (SDO) (Pesnell et al. 2012) takes images of the Sun through seven EUV channels. The AIA has a field of view (FOV) of 1.3 $R_\odot$, a spatial resolution of 1.2″ and a cadence of 12 s. Here we use the 131 Å (Fe XXI, $\sim$10 MK) and 304 Å (He II, $\sim$0.05 MK) to display the hot channel and prominence, respectively.

The K-COR is one of three proposed instruments in the COSMO facility suite (Tomczyk et al. 2016) located at the Mauna Loa Solar Observatory (MLSO), and records the coronal polarization brightness (pB) in the passband of 7200–7500 Å, which is formed by Thomson scattering of photospheric light from free electrons (Hayes et al. 2001). The FOV of K-COR is 1.05–3 $R_\odot$ with a pixel size of 5.5″ and a nominal cadence of 15 s. The Large Angle and Spectrometric Coronagraph (LASCO; Brueckner et al. 1995) on board the Solar and Heliospheric Observatory (SOHO; Domingo et al. 1995) comprises of three telescopes (C1, C2 and C3), each of which has an increasingly large FOV. Here the C2 (FOV: 2–6 $R_\odot$) is adopted to observe the CME structure in the outer corona.

The images of space-borne LASCO/C2 have better contrast than those of the ground-based K-COR. The normalized radially graded filter (NRGF) is employed to increase the K-COR contrast, which flattens the steep brightness gradient of the corona (Morgan et al. 2006). In this paper, we examine the CME structure through the NRGF data of K-COR that are available online[1], while for the C2 observations the original data are used.

3. OBSERVATIONS AND RESULTS

The K-COR data are available since 2013 September 30, while the coronagraph is closed temporarily due to the volcanic eruption of Mauna Loa on 2022 November

---

[1] www2.hao.ucar.edu/mlso/mlso-home-page

27. Therefore, our survey covers an interval from 2013 to 2022, during which 369 CMEs (excluding the possible events) are identified. On the whole, more CMEs are recorded around solar maximum though the K-COR does not work 24 hours continuously. The basic information for each event, such as the date, time (Universal Time, UT), and location (E–east, S–south, W–west, and N–north), is listed on the MLSO website. After inspecting the 369 CMEs combining observations of the AIA, K-COR and C2, we find 71 events according to the criteria: 1) limb event, which requires that the source region centered within 30° of the solar limb for the front-side events. For the far-side events, a limb event requires that the suspended prominence (or hot channel) prior to the eruption or the coronal disturbance (or post eruption arcade) during the eruption can be observed with the AIA; 2) normal CME, i.e., angular width ≥ 30° in the C2 FOV; 3) K-COR caught the early eruption stage.

We first scrutinize the 71 CMEs one by one through the NRGF images of K-COR, and find that all of them have the three-part feature in the low corona, irrespective of their appearance in the C2 images, agreeing with the prediction of the new explanation on the three-part structure of CMEs. However, visual identification of the three-part feature is not entirely objective as no quantitative criteria. There exist 6 events that do not have the clear three-part feature in the K-COR images (See Table 1), and several or all of them might be identified as the non-three-part CMEs. Therefore, we suggest that 90–100% of the 71 CMEs possess the three-part structure in the low corona.

Table 1 lists the information of the 71 CMEs. The first column is the sequential number. Columns 2–4 give the date, time, and location of each event, which are from the MLSO website. The asterisks in Column 2 denote the 6 ambiguous events in the K-COR images mentioned above. Combining the observations of K-COR and AIA, we identify the type of source region, i.e., active region (AR) or quiet-Sun region (QS), and the ejecta, i.e., hot channel (HC) or prominence (P) for each event. The source type and ejecta are listed in Columns 5 and 6, respectively, where the "?" denotes that the source-region type or the ejecta are unsure, mainly because the events are located on the far side of the Sun. The subsequent four columns present CME information observed with LASCO, which are provided by the coordinated data analysis workshops (CDAW[2]). Column 7 is the time of the CME's first appearance in the C2 FOV, and Columns 8–10 are the central position angle (PA), linear velocity (LV), as well as angular width (AW) correspondingly. The last column tells whether the CME exhibits the three-part feature in the C2 FOV, with Y/N denoting yes/no. Note that the asterisks in the last column indicate the ambiguous events in the C2 images.

Table 1. The information of 71 limb CMEs in the K-COR and LASCO/C2 observations. Universal Time is used.

No.	Date (yyyymmdd)	K-Cor Time (hhmm–hhmm)	Location	Source	Ejecta	First in C2 (hh:mm:ss)	PA (°)	LV (km s^{-1})	AW (°)	Three Part in C2?
1	20140211	1845–1930	W-SW	AR	P	19:24:05	248	613	271	Y
2	20140220	2224–2250	W	AR	P	23:12:11	282	198	45	N
3	20140429	1940–0046	SW	QS	P	20:57:25	229	232	71	N
4	20140524	2108–2200	NE	AR	P	22:00:05	66	377	180	N
5	20140528	1714–2118	W-NW	QS	P	20:36:05	297	296	84	Y
6	20140614	1926–1940	E-SE	AR	HC	19:48:28	89	732	139	N
7	20140626	2114–0000	NE	AR	HC	21:48:57	41	497	231	N*
8	20140630	1733–1848	SW	QS	P	18:36:05	261	262	72	N
9	20140923	2336–2349	NE	AR	HC	00:48:05	68	311	52	N
10	20141014	1836–2002	E-SE	AR	HC	18:48:06	90	848	360	Y
11	20141105	1923–1950	E-NE	AR	HC	19:48:05	76	608	203	N

Table 1 *continued*

Table 1 *(continued)*

No.	Date (yyyymmdd)	K-Cor Time (hhmm–hhmm)	Location	Source	Ejecta	First in C2 (hh:mm:ss)	PA (∘)	LV (km s^{-1})	AW (∘)	Three Part in C2?
12	20141210*	1749–1958	SW	AR	P	18:00:06	322	1086	228	N
13	20141221	0048–0150	E-NE	AR	P	01:25:53	60	283	116	N
14	20141221	0152–0219	E-NE	AR	P	02:36:05	60	283	116	Y
15	20150208*	2219–2250	E	AR	P	22:36:06	100	315	132	N
16	20150425	1803–1900	W-NW	AR	P	18:48:05	304	493	50	N
17	20150501*	2156–2228	SW	AR?	P	22:12:05	264	253	83	N
18	20150505	2209–2300	NE	AR	P	22:24:05	41	715	360	N
19	20150516	0101–0200	NE	QS	P	00:12:06	42	600	177	Y
20	20150525	2110–0045	E	QS	P	23:12:11	81	374	120	N*
21	20150702	1712–1904	NE	AR?	P	17:48:04	58	629	161	Y
22	20150801	1704–2200	NE	QS	P	17:36:04	65	472	67	N
23	20150923	1800–2000	SE	QS	P	18:36:04	106	565	99	Y
24	20151217	1922–2300	NE	QS	P	20:57:28	74	137	83	N
25	20160101	2256–2350	SW	AR	P	23:24:04	227	1730	360	Y
26	20160115	1940–2158	SW	AR	HC?	20:36:04	247	292	95	N
27	20160208	2220–0032	NE	QS	P	22:00:06	18	311	164	Y
28	20160209	1758–2050	E	QS	P	19:23:30	72	358	76	N
29	20160611	2206–2238	E-NE	AR	P	23:24:05	68	95	32	N
30	20160808	2022–2100	W	AR?	HC?	20:48:06	260	674	84	Y
31	20160808	1900–0130	W-NW	QS?	P?	01:25:43	311	128	66	N*
32	20160929	1718–2050	SW	AR	HC	20:12:05	254	447	125	Y
33	20170128*	1928–0216	W	AR	HC	21:48:05	280	562	53	N
34	20170327	1732–2010	E	AR	HC	18:12:05	89	230	46	N
35	20170402	1844–2020	W-NW	AR	HC	19:24:05	290	500	88	N
36	20170713	2008–2026	W	AR	P	20:36:05	260	290	61	N
37	20170720	1700–1902	W	AR?	P?	18:12:05	265	590	95	Y
38	20170820	1934–2104	E	AR	HC	20:24:05	88	207	43	N
39	20170912	1858–1941	W-SW	AR?	HC?	19:12:05	271	476	113	Y
40	20171020	2328–0014	SE	AR	P	00:00:05	98	331	109	N
41	20190422*	0254–0422	W-NW	QS?	P	03:24:05	269	422	55	N
42	20201101	1900–2020	SW	AR	HC	19:48:05	266	289	36	N
43	20201126	2020–2105	NE	AR	HC	21:12:10	99	572	92	Y
44	20210429	1701–2146	NE	QS	P	20:01:34	75	189	129	N*
45	20210507	1852–2005	E	AR	HC	19:24:05	76	754	114	N
46	20210610	1746–1904	E-NE	AR?	P	18:24:05	83	833	133	Y
47	20210625	2017–0145	SW	QS	P	00:48:05	234	101	30	N
48	20210626	2132–0210	W-NW	AR	P	03:48:05	247	223	115	N
49	20210715	2110–2344	SE	QS	P	21:36:05	166	1476	360	Y
50	20210719*	2022–2122	E	AR	HC	20:57:05	69	401	133	N*
51	20210829	1956–2040	SW	AR	P	20:24:05	259	1060	87	N

Table 1 *continued*

Table 1 *(continued)*

No.	Date (yyyymmdd)	K-Cor Time (hhmm–hhmm)	Location	Source	Ejecta	First in C2 (hh:mm:ss)	PA (∘)	LV (km s⁻¹)	AW (∘)	Three Part in C2?
52	20211009	2030–0125	W-NW	AR	HC	22:36:05	275	433	110	Y
53	20211010	2235–0150	NW	AR	P	23:24:05	293	299	71	N
54	20211102	2130–2353	SE	AR	HC	22:24:05	113	474	98	N
55	20211103	2050–2216	W-SW	AR	P	21:36:05	260	510	360	N
56	20220131	2328–0001	SW	QS	P	00:12:05	245	469	52	N
57	20220201	2300–0213	SW	QS	P	01:25:48	243	467	43	N*
58	20220419	2043–2204	W-SW	AR	HC	21:24:05	227	247	53	N
59	20220425	1723–1854	SE	AR	P	18:00:05	85	319	120	N
60	20220425	1836–2131	SE	AR	P	20:24:05	90	498	125	Y
61	20220508	2124–2250	SE	AR	HC	22:24:05	94	602	175	Y
62	20220511	1820–1950	W	AR	P	18:36:05	237	1100	194	N
63	20220514	1653–2106	SE	QS	P	18:24:05	115	843	52	N
64	20220524	2219–2324	NE	AR	P	23:12:11	71	569	211	Y
65	20220710	1658–1931	SW	QS	P	17:48:05	198	1241	43	N
66	20220731	2236–0010	E	AR	P	23:12:10	82	1122	192	N
67	20220830	1744–1927	S-SW	AR	HC	18:12:05	268	1247	360	Y
68	20220924	1957–2339	SE	QS	P	20:24:05	132	337	103	N*
69	20220928	1718–1818	E	AR	P	17:36:05	87	256	115	N
70	20221026	1900–2231	SW	QS	P	21:12:09	207	506	167	N
71	20221125	2128–2356	NW	QS	P	22:24:05	312	620	106	N

Table 1 shows that 49 and 22 CMEs originate from active regions (AR) and quiet-Sun regions (QS), respectively. For the ejecta type, there are 49 events associated with a prominence (P) eruption, and the rest are correlated with a hot-channel (HC) eruption. In the LASCO FOV, the linear velocities range from 95 to 1730 km s⁻¹, and their angular widths, from 30 to 360°. After scrutinizing the 71 CMEs one by one through the C2 images, we find that only 21 events (∼30%) possess the three-part structure, agreeing with previous statistical results based on C2 observations (e.g., Vourlidas et al. 2013). For the 50 non-three-part CMEs in the C2 images, 7 ones are ambiguous and might be identified as the three-part events, which are denoted with asterisks in the last column as mentioned. Therefore, we suggest that 30–40% of the 71 CMEs possess the three-part structure in the high corona. To demonstrate that a hot channel or prominence can lead to a three-part CME in its early eruption stage, and the three-part feature can sustain or disappear in the outer corona, we select four representative events and display them in Figures 1–4 sequentially.

Figure 1 displays the event occurring on 2014 October 14 (Event 10 in Table 1), which resulted from a hot-channel eruption in an active region located at the SE limb. Panel (a) shows the hot channel with the AIA 131 Å observation at 18:45:32 UT. Panel (b) presents the K-COR observation at 18:58:51 UT, and the three-part CME can be identified. The bright core is very obvious, and the bright front is delineated with the red-dashed line as we can not discern the front clearly in the static image. The bright front and three-part structure can be distinguished clearly through the animation accompanying with Figure 1. The C2 image at 20:00:05 UT is presented in Panel (c), and we can see that the CME keeps the typical three-part feature there. Note that the white circles in both Panels (b) and (c) denote the solar limb.

Figure 2 presents the CME occurring on 2016 January 1 (Event 25 in Table 1). This event is associated with a prominence eruption that can be observed in the AIA 304 Å image as shown in Panel (a). Panel (b) displays the K-COR observation at 23:23:42 UT, in which the bright front and core are delineated with the red- and yellow-dashed lines, respectively, to display the three-part structure clearly. Please see the accompanied animation to examine the three-part feature continuously. This CME also exhibits the three-part feature in the C2

FOV as shown in Panel (c), where the red-dashed line denotes the leading front.

The above two CMEs exhibit the three-part structure in both K-COR and C2 images. Next we'll show two events that do not have the three-part feature in the C2 FOV. Figure 3 displays a CME induced by the hot-channel eruption as revealed with the AIA 131 Å observation in Panel (a). This event occurred on 2021 May 7 (Event 45 in Table 1) and a previous study (Wang et al. 2022) has demonstrated that the hot channel evolved into the bright core in the K-COR image as shown in Panel (b). The three-part feature is distinguishable directly in the static image, thus no dashed lines are guide for the eye in this panel. Panel (c) shows the observation of C2 at 19:48:05 UT with the red-dashed line delineating the CME front. The CME lost its three-part feature due to the MFR expansion and growth as mentioned (Song et al. 2019a, 2023).

Figure 4 shows the CME occurring on 2021 October 10 (Event 53 in Table 1), which is associated with the prominence eruption from an active region located at the NW limb. Panel (a) illustrates the erupting prominence with the AIA 304 Å image at 22:51:29 UT. The K-COR observations present a typical three-part CME as shown in Panel (b), where the red-dashed line depicts the CME front. Please see the accompanied animation to view the three-part feature in the K-COR images. The animation also demonstrates that the prominence did not erupt outward eventually. This leads to a non-three-part CME in the C2 image (Song et al. 2023) as presented in Panel (c), where the red-dashed line delineates the CME front.

4. SUMMARY AND DISCUSSION

To verify the new explanation on the three-part structure of CMEs, which predicts that all normal CMEs should exhibit the three-part feature in their early eruption stage, we conducted a survey study on the CME structure with the observations of K-COR (FOV: 1.05–3 $R_\odot$) at MLSO. In total, 369 CMEs (excluding the possible events) are identified from 2013 September to 2022 November. Combining the observations of AIA, K-COR and LASCO/C2, we inspected the events one by one manually, and found 71 events according to the criteria: 1) limb event; 2) normal CME with angular width $\geq 30°$ in the C2 FOV (2–6 $R_\odot$); 3) K-COR caught the early eruption stage. The results showed that 90–100% of the 71 events exhibit the three-part structure in the K-COR observations, basically agreeing with the prediction of the new explanation, and 30–40% of the events have the three-part appearance in the C2 observations, consistent with previous survey studies (e.g., Vourlidas et al. 2013; Song et al. 2023). These suggest

that CMEs can lose the three-part feature during their propagation outwards, and further support the new explanation on the nature of the three-part structure of CMEs(Song et al. 2022).

As mentioned, theoretical studies demonstrate that CMEs result from MFR eruption, and no physical mechanism can produce large-scale CMEs without involving an MFR. However, do all CMEs have an MFR structure near the Sun observationally? Our current survey study intends to answer "Yes" to this question, as 90–100% of normal CMEs exhibit the three-part structure in their early eruption stage. We think that the several ambiguous events could exhibit the three-part feature if the observations were clearer. For the narrow CMEs (angular width $< 30°$), we speculate that they can also exhibit the three-part feature when the spatial resolution of coronagraphs is high enough.

The CME and MFR are called ICME (interplanetary CME) and magnetic cloud (Burlaga et al. 1981), respectively, after they leave the corona. If the MFR structures are not destroyed during their propagation, all ICMEs should possess the magnetic cloud features near 1 au, such as enhanced magnetic-field intensity, large and smooth rotation of the magnetic-field direction, and low proton temperature or low plasma β (Zurbuchen & Richardson 2006; Wu & Lepping 2011; Song & Yao 2020). However, only about one third of ICMEs have the magnetic cloud features near the Earth (Chi et al. 2016). From the statistical point of view, this might be a result of glancing cuts between the spacecraft and ICME, as ICMEs with magnetic cloud features have narrower sheath region compared to the non-cloud ICMEs (Song et al. 2020). The analyses on the morphological structure of CMEs near the Sun and the geometric character of ICMEs near 1 au support that most (if not all) CMEs have the MFR structures.

REFERENCES

Brueckner, G. E., Howard, R. A., Koomen, M. J., et al. 1995, SoPh, 162, 357, doi: 10.1007/BF00733434

Burlaga, L., Sittler, E., Mariani, F., & Schwenn, R. 1981, J. Geophys. Res., 86, 6673, doi: 10.1029/JA086iA08p06673

Chen, P. F. 2009, ApJL, 698, L112, doi: 10.1088/0004-637X/698/2/L112

Chen, P. F. 2011, Living Reviews in Solar Physics, 8, 1, doi: 10.12942/lrsp-2011-1

Chen, Y., Tian, H., Su, Y., et al. 2018, ApJ, 856, 21, doi: 10.3847/1538-4357/aaaf68

Cheng, X., Zhang, J., Ding, M. D., et al. 2013, ApJL, 769, L25, doi: 10.1088/2041-8205/769/2/L25

Chi, Y., Shen, C., Wang, Y., et al. 2016, SoPh, 291, 2419, doi: 10.1007/s11207-016-0971-5

Domingo, V., Fleck, B., & Poland, A. I. 1995, SoPh, 162, 1, doi: 10.1007/BF00733425

Follett, W. H., Ostwald, L. T., Simpson, J. O., & Spencer, T. M. 1974, Journal of Spacecraft and Rockets, 11, 327, doi: 10.2514/3.62071

Forland, B. C., Gibson, S. E., Dove, J. B., Rachmeler, L. A., & Fan, Y. 2013, SoPh, 288, 603, doi: 10.1007/s11207-013-0361-1

Gibson, S. E., Foster, D., Burkepile, J., de Toma, G., & Stanger, A. 2006, ApJ, 641, 590, doi: 10.1086/500446

Gopalswamy, N., Shimojo, M., Lu, W., et al. 2003, ApJ, 586, 562, doi: 10.1086/367614

Hayes, A. P., Vourlidas, A., & Howard, R. A. 2001, ApJ, 548, 1081, doi: 10.1086/319029

Howard, R. A. 2006, Geophysical Monograph Series, 165, 7, doi: 10.1029/165GM03

Howard, T. A., DeForest, C. E., Schneck, U. G., & Alden, C. R. 2017, ApJ, 834, 86, doi: 10.3847/1538-4357/834/1/86

Illing, R. M. E., & Hundhausen, A. J. 1985, J. Geophys. Res., 90, 275, doi: 10.1029/JA090iA01p00275

Jiang, C., Feng, X., Liu, R., et al. 2021, Nature Astronomy, 5, 1126, doi: 10.1038/s41550-021-01414-z

Kliem, B., Lee, J., Liu, R., et al. 2021, ApJ, 909, 91, doi: 10.3847/1538-4357/abda37

Koomen, M. J., Detwiler, C. R., Brueckner, G. E., Cooper, H. W., & Tousey, R. 1975, ApOpt, 14, 743, doi: 10.1364/AO.14.000743

Lemen, J. R., Title, A. M., Akin, D. J., et al. 2012, SoPh, 275, 17, doi: 10.1007/s11207-011-9776-8

Li, L. P., Zhang, J., Li, T., Yang, S. H., & Zhang, Y. Z. 2012, A&A, 539, A7, doi: 10.1051/0004-6361/201015796

Low, B. C. 2001, J. Geophys. Res., 106, 25141, doi: 10.1029/2000JA004015

Morgan, H., Habbal, S. R., & Woo, R. 2006, SoPh, 236, 263, doi: 10.1007/s11207-006-0113-6

Ouyang, Y., Yang, K., & Chen, P. F. 2015, ApJ, 815, 72, doi: 10.1088/0004-637X/815/1/72

Patsourakos, S., Vourlidas, A., & Stenborg, G. 2013, ApJ, 764, 125, doi: 10.1088/0004-637X/764/2/125

Pesnell, W. D., Thompson, B. J., & Chamberlin, P. C. 2012, SoPh, 275, 3, doi: 10.1007/s11207-011-9841-3

Song, H., Li, L., & Chen, Y. 2022, ApJ, 933, 68, doi: 10.3847/1538-4357/ac7239

Song, H., & Yao, S. 2020, Sci China Tech Sci, 63, 2171, doi: 10.1007/s11431-020-1680-y

Song, H., Zhang, J., Li, L., et al. 2023, ApJ, 942, 19, doi: 10.3847/1538-4357/aca6e0

Song, H. Q., Chen, Y., Qiu, J., et al. 2018, ApJL, 857, L21, doi: 10.3847/2041-8213/aabcc3

Song, H. Q., Chen, Y., Zhang, J., et al. 2015a, ApJL, 808, L15, doi: 10.1088/2041-8205/808/1/L15

Song, H. Q., Zhang, J., Chen, Y., & Cheng, X. 2014, ApJL, 792, L40, doi: 10.1088/2041-8205/792/2/L40

Song, H. Q., Zhang, J., Chen, Y., et al. 2015b, ApJ, 803, 96, doi: 10.1088/0004-637X/803/2/96

Song, H. Q., Zhang, J., Cheng, X., et al. 2019a, ApJ, 883, 43, doi: 10.3847/1538-4357/ab304c

Song, H. Q., Zhang, J., Li, L. P., et al. 2019b, ApJ, 887, 124, doi: 10.3847/1538-4357/ab50b6

Song, H. Q., Cheng, X., Chen, Y., et al. 2017, ApJ, 848, 21, doi: 10.3847/1538-4357/aa8d1a

Song, H. Q., Zhang, J., Cheng, X., et al. 2020, ApJL, 901, L21, doi: 10.3847/2041-8213/abb6ec

Tomczyk, S., Landi, E., Burkepile, J. T., et al. 2016, Journal of Geophysical Research (Space Physics), 121, 7470, doi: 10.1002/2016JA022871

Tousey, R. 1973, in Space Research XIII, ed. M. J. Rycroft & S. K. Runcorn (Berlin: Akademie-Verlag), 713 https://ui.adsabs.harvard.edu/abs/1973spre.conf..713T/abstract

Vourlidas, A., Lynch, B. J., Howard, R. A., & Li, Y. 2013, SoPh, 284, 179, doi: 10.1007/s11207-012-0084-8

Wang, B. T., Cheng, X., Song, H. Q., & Ding, M. D. 2022, A&A, 666, A166, doi: 10.1051/0004-6361/202244275

Wang, W., Liu, R., Wang, Y., et al. 2017, Nature Communications, 8, 1330, doi: 10.1038/s41467-017-01207-x

Wang, Y. M., & Stenborg, G. 2010, ApJL, 719, L181, doi: 10.1088/2041-8205/719/2/L181

Webb, D. F., & Howard, T. A. 2012, Living Reviews in Solar Physics, 9, 3, doi: 10.12942/lrsp-2012-3

Wu, C.-C., & Lepping, R. P. 2011, SoPh, 269, 141, doi: 10.1007/s11207-010-9684-3

Yan, X. L., Priest, E. R., Guo, Q. L., et al. 2016, ApJ, 832, 23, doi: 10.3847/0004-637X/832/1/23

Zhang, J., Cheng, X., & Ding, M.-D. 2012, Nature Communications, 3, 747, doi: 10.1038/ncomms1753

Zhou, Y., Ji, H., & Zhang, Q. 2023a, SoPh, 298, 35, doi: 10.1007/s11207-023-02126-5

Zhou, Z., Jiang, C., Song, H., et al. 2023b, ApJ, 944, 175, doi: 10.3847/1538-4357/acb6f8

Zurbuchen, T. H., & Richardson, I. G. 2006, SSRv, 123, 31, doi: 10.1007/s11214-006-9010-4
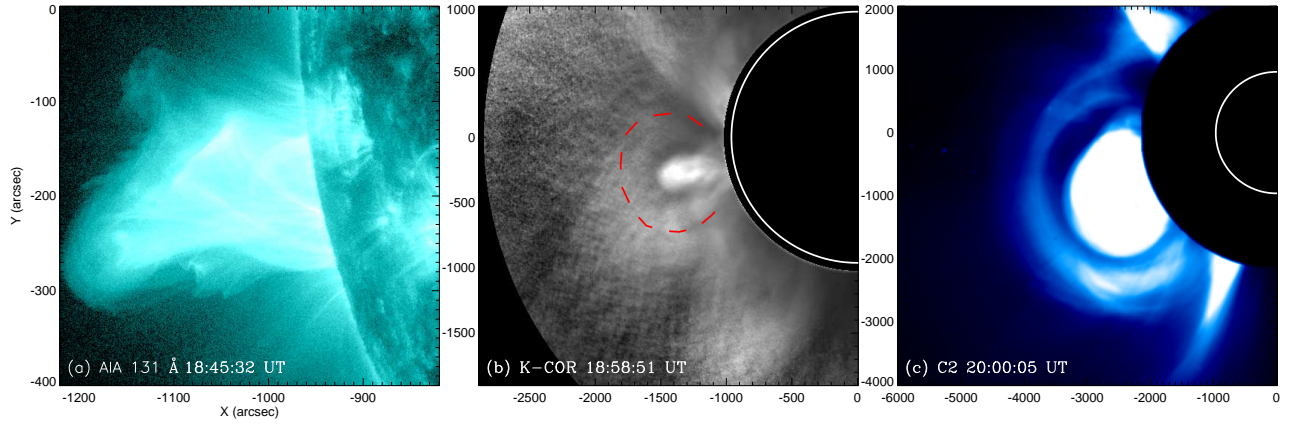
Figure 1. Observations of the CME occurred on 2014 October 14. (a) AIA 131 Å image, showing the erupting hot channel at 18:45:32 UT. (b) NRGF image of K-COR at 18:58:51 UT, displaying the three-part structure in the low corona. The animation accompanying with this panel demonstrates the complete eruption process from 18:30:32 to 20:01:34 UT. The duration of the animation is 4 s. (c) LASCO/C2 observation at 20:00:05 UT, displaying the CME structure in the high corona. The white circles in both Panels (b) and (c) denote the solar limb. The red-dashed line delineates the CME front.
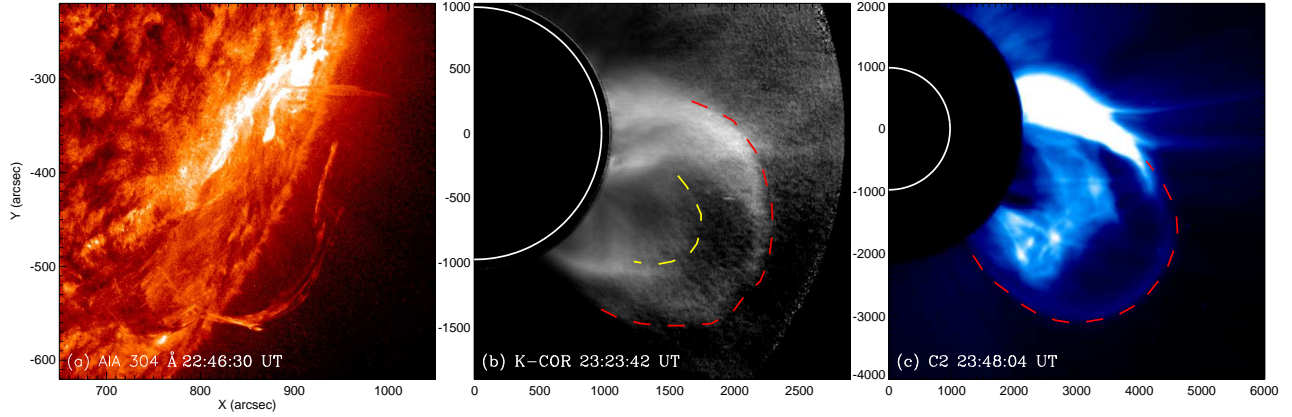

Figure 2. Observations of the CME occurred on 2016 January 1. (a) AIA 304 Å image, showing the erupting prominence at 22:46:30 UT. (b) NRGF image of K-COR at 23:23:42 UT, displaying the three-part structure in the low corona. The animation accompanying with this panel demonstrates the complete eruption process from 22:49:34 to 23:51:31 UT. The duration of the animation is 2 s. (c) LASCO/C2 observation at 23:48:04 UT, displaying the CME structure in the high corona. The white circles in both Panels (b) and (c) denote the solar limb. The red-dashed line delineates the CME front, and the yellow-dashed line, the CME core.
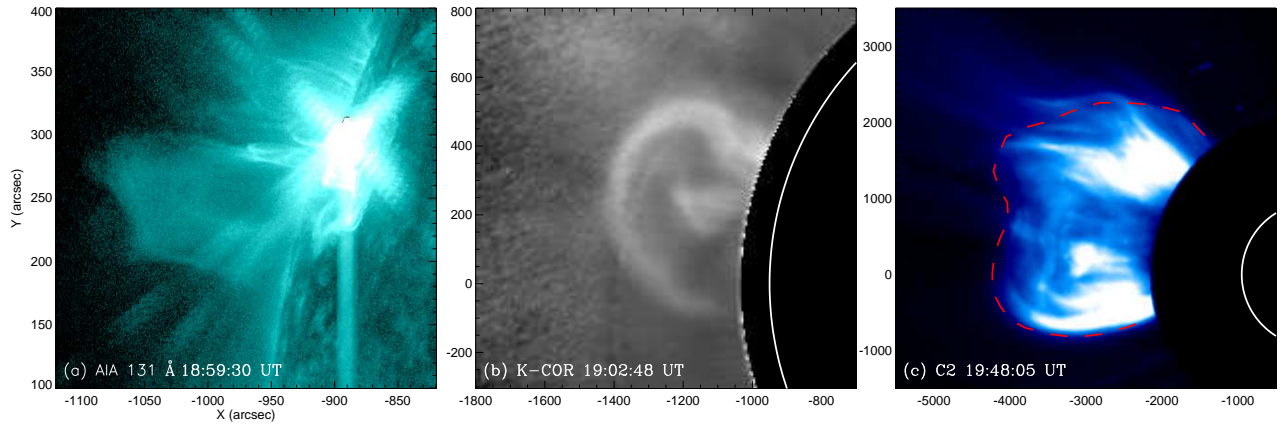
Figure 3. Observations of the CME occurred on 2021 May 7. (a) AIA 131 Å image, showing the erupting hot channel at 18:59:30 UT. (b) NRGF image of K-COR at 19:02:48 UT, displaying the three-part structure in the low corona. The animation accompanying with this panel demonstrates the complete eruption process from 18:50:40 to 19:51:21 UT. The duration of the animation is 3 s. (c) LASCO/C2 observation at 19:48:05 UT, displaying the CME structure in the high corona. The white circles in both Panels (b) and (c) denote the solar limb. The red-dashed line delineates the CME front.
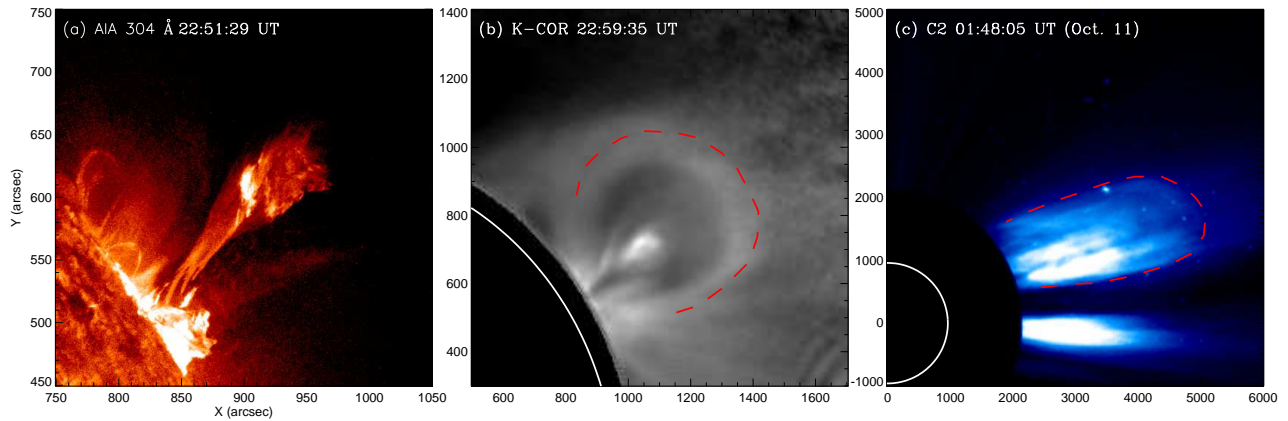

Figure 4. Observations of the CME occurred on 2021 October 10. (a) AIA 304 Å image, showing the erupting prominence at 22:51:29 UT. (b) NRGF image of K-COR at 22:59:35 UT, displaying the three-part structure in the low corona. The animation accompanying with this panel demonstrates the complete eruption process from 22:28:08 to 23:50:09 UT. The duration of the animation is 4 s. (c) LASCO/C2 observation at 01:48:05 UT on October 11, displaying the CME structure in the high corona. The white circles in both Panels (b) and (c) denote the solar limb. The red-dashed line delineates the CME front.